

Seasonal Variability of the East China/Yellow Sea Surface Fluxes and Thermohaline Structure

Peter Chu and Akira Kuninaka

Naval Ocean Analysis and Prediction Laboratory, Department of Oceanography
Naval Postgraduate School, Monterey, California, U.S.A

Yuchun Chen

Institute of Cold and Arid Environment and Engineering
Chinese Academy of Sciences, Lanzhou, China

Abstract

We use the U.S. Navy's Master Oceanographic Observation Data Set (MOODS) for the Yellow Sea/East China Sea (YES) and to investigate the climatological water mass features and the seasonal and non-seasonal variabilities of the thermohaline structure, and use the Comprehensive Ocean-Atmosphere Data Set (COADS) from 1945 to December 1989 to investigate the linkage between the fluxes (momentum, heat, and moisture) across the air-ocean interface and the formation of the water mass features. After examining the major current systems and considering the local bathymetry and water mass properties, we divide YES into five regions: East China Sea (ECS) shelf, Yellow Sea (YS) Basin, Cheju bifurcation (CB) zone, Taiwan Warm Current (TWC) region, Kuroshio Current (KC) region. The long term mean surface heat balance corresponds to a heat loss of 30 W m^{-2} in the ESC and CB regions, a heat loss of 65 W m^{-2} in the KC and TWC regions, and a heat gain of 15 W m^{-2} in the YS region. The surface freshwater balance is defined by precipitation minus evaporation. The annual water loss from the surface for the five subareas ranges from 1.8 to 4 cm mon^{-1} . The fresh water loss from the surface should be compensated from the river run-off. The entire water column of the shelf region (ECS, YS, and CB) undergoes an evident seasonal thermal cycle with maximum values of temperature during summer and maximum mixed layer depths during winter. However, only the surface waters of the TWC and KC regions exhibit a seasonal thermal cycle. We also found two different relations between surface salinity and Yangtze River run-off, namely, off-phase in the East China Sea shelf and in-phase in the Yellow Sea. This may confirm an earlier study by Beardsley et al. (1985) that the summer fresh water discharge from the Yangtze River forms a relatively shallow, low salinity plume-like structure extending offshore on average towards the northeast.

1. Introduction

The combined Yellow Sea and East China Sea (called YES) covers roughly 1,250,000 km² and is one of the most developed continental shelf areas in the world (Yanagi and Takahashi, 1993). While the Yellow Sea (YS) covers a relatively large area, it is quite shallow reaching a maximum depth of about 140 m (Figure 1). The water depth over most of the area is less than 50 m. The deepest water is confined to a north-south oriented trench which runs from the northern boundary south to the 100 m isobath where it fans out onto the continental shelf break. The bathymetric gradients are very small. Such a broad and shallow continental shelf sea suggests that the water column will be readily affected by seasonally varying atmospheric conditions such as heating, cooling, and wind stress. Therefore, the seasonal variation of the water masses is remarkably large. Another feature of the depth distribution is the east/west asymmetry. Extensive shoals (< 20 m) are located in the western Yellow Sea along the Chinese coast but are not generally found off the South Korea coastal regions. Also, the 50 m isobath is located more than 100 km from the Chinese coast, but only about 50 km from the South Korea coast. This asymmetry in bottom depth is important in controlling the mixed layer depth (Chu et al., 1997b).

The East China Sea (ECS) is located south of the YS to the north of Taiwan (Figure 1). The ECS is usually defined as reaching from the northern end of Taiwan Strait to the southern end of Kyusyu where it adjoins the YS along a line from Kyushu to Shanghai (the mouth of the Yangtze River). With the exception of the Okinawa Trough west of the Ryukyu Islands, which reaches 2,700 m depth, the ECS is part of the continental shelf. The hydrographic character of the water masses in YES depends on the bathymetry, the Kuroshio Current, the atmospheric forcing (monsoon winds, heat and moisture fluxes), and the degree of mixing of fresh water originating from Asian river runoff with the intrusion of Kuroshio waters (Tomczak and Godfrey, 1994).

To examine the seasonal variability of the water mass and circulation, we use the U.S. Navy's Master Oceanographic Observation Data Set (MOODS) to investigate the climatological features and the seasonal and non-seasonal variability of the thermohaline structure, and use the Comprehensive Ocean-Atmosphere Data Set (COADS) from 1945 to December 1989 to investigate the linkage between the fluxes (momentum, heat, and moisture) across the air-ocean interface and the formation of the water mass features.

2. YES Oceanography and Subdivision

2.1. Water Masses

Earlier studies (e.g., Liu et al., 1992; Su and Weng, 1994, Chen et al., 1995) have shown that a complex water mass structure exists in YES based on temperature and salinity features. The water in the shallow parts of YES is affected greatly by the atmospheric and geographic conditions, and therefore it does not have the homogeneity as in the open ocean. Su and Weng (1994) proposed a concept of modified water mass holding similar physical and chemical characteristics and occupying a certain space.

Based on temperature data observed in 1978-1980, Su et al. (1983) identified the following water masses using a successive clustering method on temperature observations: Kuroshio Surface Water (KSW), East China Sea Mixed Water (ECSMW), East China Sea Deep Water (ECSDW), Yellow Sea and East China Sea Mixed Water (YEMW), Yellow Sea Mixed Water (YSMW), Yellow Sea Bottom Cold Water (YSCW), Yellow Sea Near-shore Water (YSNW), and Continental Shelf Diluted Water (CSDW).

Since salinity is a more conserved quantity in the YES than temperature (Su and Weng, 1994), the water masses are classified into three systems based on their salinity features: (i) the ECS water system (or the open water system), including KSW, ECSMW, ECSDW, and YEMW (in

May only) and originated from the Kuroshio Water Mass, (ii) the YS water system (or the local water system), including YSMW, YSCW, YEMW, and (iii) coastal water system, including CSDW and YSNW.

Since the ECS water system is an open water system, horizontal advection, especially meandering of the Kuroshio Current, should be an important factor in its variability. In contrast, the YS water system is a local system. The local atmospheric forcing should be responsible for its variability. In fact, the central region of the YS stands out due to its cold bottom water, that is YSCW. During summer, strong surface warming generates the sharpest thermocline on the top of the YSCW in the region. During winter, this water mass provides a significant buffer preventing central YS water temperatures from reaching the near-freezing temperatures that the near-shore regions experience (Chu et al. 1997a, b).

2.2. Subdivision

After examining the major current systems, water mass structure, and considering the local bathymetry and water mass properties, we have divided the YES into five regions (Figure 2): (1) the ECS shelf with the eastern boundary at the 80 m bathymetry contour line and the northern boundary at 32°N, representing the coastal current system; (2) the YS shelf with the northern boundary at 38°30'N, the southern boundary at 32°N, the western boundary at 122°E in the mouth of Gulf of Bohai and the Chinese coast, and the eastern boundary at the Korean coast and 80m depth contour line, representing the YS gyre system; (3) the Cheju bifurcation (CB) area with the northern and western boundaries at 80m contour, the eastern boundary at 127°15'E, and the southern boundary at 32°N, representing the TWC branching into Tsushima Current and Yellow Sea Warm Current; (4) the Taiwan Warm Current area bounded by the 80 m and 200 m

bathymetric contours, and 32°N latitude, representing the TWC system; and (5) the Kuroshio area bounded by 200m and 4000m contours, and 32°N latitude, representing the KC system.

3. Seasonal Variation of the Atmospheric Forcing

3.1 General Description

The Asian monsoon strongly affects the thermal structure of YES. During the winter monsoon season, a very cold northwest wind blows over the ECS/YS as a result of the Siberian High Pressure System. The Jet Stream is positioned to the south of the YS and the Polar Front to the north of the Philippines. By late April the Polar Front has moved northward toward Korea with warm, moist air following behind. Numerous frontally-generated events occur making late April and May highly variable in terms of wind speeds and cloud amount. During this period storms originating in Mongolia may cause strong, warm westerlies carrying yellow desert sand (termed the "Yellow Wind"). By late May and early June the summer surface atmospheric low pressure system begins to form over Asia. Initially this low pressure system is centered north of the Yellow Sea producing westerly winds. In late June this low begins to migrate to the west setting up the southwest monsoon that dominates the summer months. The winds remain variable through June until strengthening of the Manchurian Low pressure system occurs. The Jet Stream migrates just south of Korea, and the Polar Front is just south of Kyushu and Shikoku. Despite the very active weather systems, the mean surface wind speed over the central Yellow Sea in summer is between 3 and 4 m s⁻¹, which is weaker than in winter. June also marks, historically, a jump in precipitation associated with warm, moist air south of the Polar Front (Watts, 1969). Occasionally the Okhotsk High blocks the northerly progression of the Polar Front. By July, however, high pressure (the Bonin High) to the south and the low pressure over Manchuria produce southerly winds carrying warm, moist air over YES.

The summer monthly mean surface air temperature (SAT) is usually 1.5-2°C warmer than the mean sea surface temperature (SST) (Van Loon, 1984). The warmer air causes a downward heat flux at the air-ocean interface. This heat flux plus the strong downward net radiation stabilizes the upper layer of the water and causes the surface mixed layer to shoal, creating a multi-layer structure. Below the thermocline in the YS, there is a cold water mass, commonly referred to as Yellow Sea Bottom Cold Water (YSCW) that remains unchanged and nearly motionless throughout the summer (Li and Yuan, 1992). October is the beginning of the transition back to the winter conditions. The southerly winds weaken letting the sea surface slope reestablish the winter pattern. The YS SST steadily decreases from 12°C in October to 4°C in January (Chu et al., 1997a).

3.2 Surface Climatology

Here, we present a climatological description of the atmospheric conditions over YES and their effect in terms of heat exchange and storage, derived from the COADS data (1945-1989) on 1° resolution. The climatological monthly mean values of wind speed, temperature and relative humidity are shown in Figures 3a-c for the months of February, May, August, and November, which may be regarded as representative patterns for each season.

The main characteristic of the COADS wind data (Figure 3a) is the seasonal variation of the monsoon winds. In winter, strong north to northwest winds prevail in the northern YES and north to northeast winds prevail in the southern YES. In summer, weak southeast winds prevail. May is the summer monsoon transition period. The surface winds over the YS are very weak (mean monthly wind speed less than 3 m/s) both in summer and during the summer monsoon transition period.

The SAT exhibits seasonal fluctuations of about 22°C in the YS and about 10°C in the ECS, averaging about 17°C over the entire domain (Figure 3b). A nearly latitudinal gradient prevails in

all seasons with the maximum south-to-north mean SAT difference of 18°C in February and the minimum SAT difference of 3°C in August. The SAT is uniformly warm (mean SAT around 28°C) in the ECS during summer (August).

Surface relative humidity (Figure 3c) is generally higher in the summer season, mainly as a consequence of the southeast summer monsoon bringing moisture air from tropics. The summer field is relatively homogeneous (83%) in the ECS, whereas a significant latitudinal gradient exists in rest of seasons. A relative humidity minimum (maximum) is present in all seasons near Kyushu Island (Chinese coast), which may lead to maximum (minimum) evaporation there.

3.3 Surface Fluxes

3.3.1. Net Heat Flux

Net surface heat flux (Q_{net}) is computed by

$$Q_{net} = R_S - (R_L + Q_L + Q_S) \quad (1)$$

where R_S is the net downward shortwave radiation, R_L the net upward longwave radiation, Q_L the sensible heat flux, and Q_S the latent heat flux. Positive (negative) values of Q_{net} indicate net heat gain (loss) of the ocean at the surface. The fluxes (R_S , R_L , Q_L , Q_S) are directly obtained from COADS data set. The summer field is relatively homogeneous (120-160 W/m²) in the whole YES, whereas a significant horizontal gradient with a minimum center near Kyushu Island exists in rest of seasons (Figure 4). The ocean surface near Kyushu Island (belonging to the KC and TWC sub-regions) has a maximum heat loss of 280 W m⁻² in the winter (November, February), and a minimum heat gain of 80 W/m² in the spring. This long term net surface heat loss will be compensated by the advection of warm tropical waters by KC and TWC. Besides, there is an increase of net surface heat gain (flux downward) toward the Chinese coast in all seasons, which might be caused by less evaporation there.

The annual mean heat budget is positive in the YS region (15 W/m^2) and negative elsewhere: around -30 W/m^2 in the ECS and CB regions, and -65 W/m^2 in the KC and TWC regions. A low annual mean latent heat flux in the YS region causes the positive annual heat budget. Sensible heat flux is nearly zero in summer, which implies SST close to SAT. The ratio between sensible and latent heat fluxes (defined as the Bowen ratio) is listed in the seventh column of these tables. The Bowen ratio has the following features: (a) value less than one any month for all five sub-areas, indicating larger latent heat flux than the sensible heat flux, (b) a seasonal variation with relatively large values (0.33-0.67) in winter and near zero values in summer, and (c) larger annual variation in the shallow water regions (YS, CB) than in the relatively deep water regions (KC and TWC).

The monthly variation of net surface heat flux (Figure 5) is nearly sinusoidal and quite similar among the five sub-areas. The YS region leads the rest of the sub-areas by half to one month: Q_{net} becomes positive in mid-February in the YS region, in early March in the ECS and CB regions, and in late March in the KC and TWC regions. Q_{net} peaks in June in the YS region and in July in the rest of sub-areas.

3.3.2. Fresh Water Flux

The surface fresh water flux is the difference between precipitation rate (P) and evaporation rate (E),

$$F = P - E. \quad (2)$$

Positive values of F indicate net water mass gain of the ocean at the surface. The surface fresh water flux exhibits a distinct winter and summer pattern (Figure 6). The summer pattern is characterized by fresh water gain in the whole area, and a saddle-type distribution with two low

centers, one in the east (less than 3 cm/mon near Kyushu Island) and another in the west (less than 1 cm/mon near the Chinese coast). Centers of high fresh water flux are found in the north (more than 14 cm/mon in northern YS) and in the south (8 cm/mon). The winter pattern is characterized by fresh water loss in the whole area with a maximum water mass loss (19 cm/mon in November) near Kyushu Island.

The climatological monthly surface fresh water flux components for the five sub-areas shows similar features: (a) fresh water gain during the summer monsoon season and fresh water loss during the winter monsoon season, and (b) net annual fresh water loss (1.8-4 cm/mon) from the air-ocean interface. Such a long term surface saline process might be compensated by the river runoff. The seasonal cycle of surface fresh water budget (Figure 7) shows that E exceeds P during the winter monsoon period (September to March) and P exceeds E during summer monsoon period (May to August). The shallow water region (YC, ECS, CB) leads the relatively deep region (KC, TWC) by near one month to get fresh water. F peaks in July in the YS sub-area and in June elsewhere.

3.3.3. Surface Buoyancy Flux

Both Q_{net} and F are in-phase during the seasonal variation: positive (negative) values during summer (winter) monsoon season. Thus, the surface buoyancy flux,

$$B = \frac{\alpha g Q_{net}}{\rho_w c_{pw}} + \beta g (P - E) S_0 \quad (3)$$

should have a similar seasonal variation as Q_{net} and F . Here, g is the earth gravitational acceleration, ρ_w the characteristic water density, c_{pw} the water specific heat under constant pressure, α the water thermal expansion coefficient, β the salinity contraction coefficient, and S_0 the surface salinity. The surface buoyancy flux, B , for the five sub-regions has a similar quasi-sinusoidal

seasonal variation with the maximum buoyancy gain (loss) in the summer (winter), which results in a shallow (deep) mixed layer in summer (winter).

4. Hydrographic Data Set

The MOODS is a compilation of observed ocean data worldwide consisting of (a) temperature-only profiles; (b) both temperature and salinity profiles, (c) sound-speed profiles, and (d) surface temperatures from drifting buoys. These measurements are, in general, irregular in time and space. In this study, we analyze temperature and salinity profiles measured from a variety of instruments. Due to the sheer size (more than six million profiles) and enormous influx of data to the Naval Oceanographic Office from various sources, quality control is a difficult task (Chu et al., 1997c). Our study domain lies inside the area 24° to 40° N and 118° to 132° E (Figure 8); the data set within this region consisted of nearly 24,000 profiles after rejecting certain data during quality control. These primary editing procedures included removal of profiles with obviously erroneous location, profiles with large spikes, and profiles displaying features that do not match the characteristics of surrounding profiles. In shallow water, this procedure can be partially automated but also involves subjective interpretation because of the under-sampling of MOODS compared to the spatial and temporal variability of the water masses (Chu et al., 1997a, b).

The main limitation of the MOODS data is its irregular distribution in time and space. Certain periods and areas are over sampled while others lack enough observations to provide meaningful insights. Vertical resolution and data quality are also highly variable depending much on instrument type and sampling expertise. A prominent data sparse area is located off the eastern coastal region of China (Figure 8). The period of 1975 to 1986 is found to have a relatively large number of profiles. Yearly temperature (salinity) casts above 2,000 (400) are 1975, 1976, 1978, 1981, and 1986 (Figure 9a, b). Within a given year temporally uneven distributions can be seen

such as in the 1984 temperature casts (Figure 9c) and salinity casts (Figure 9d). Spatial and temporal irregularities along with the lack of data in certain regions must be carefully weighed in order to avoid statistically-induced variability (Chu et al, 1997c).

5. Seasonal Variation of Water Mass Characteristics

5.1 Relative Heat Storage

If we are not interested in the actual heat storage values, but rather in its annual cycle, the relative heat storage (RHS) is useful to arrange our hydrographic dataset on a seasonal basis. The definition of RHS is taken from Hecht et al. (1985),

$$\begin{aligned}
 RHS &= \frac{D}{H} \int_{-H}^0 c_p \rho_w (T - T_0) dz, & \text{if } H < D \\
 RHS &= \int_{-H}^0 c_p \rho_w (T - T_0) dz, & \text{if } H \geq D
 \end{aligned} \tag{4}$$

where H is the actual water column depth, D the maximum water depth considered, T the water temperature, and T_0 an arbitrary reference temperature. In our computations, $D = 50$ m, and $T_0 = 5^\circ\text{C}$.

The RHS values for the five sub-areas are shown in Figure 10. Two extreme seasons can be clearly identified, namely, winter from January to April, and summer from July to November. We can also define the two transition seasons: spring, consisting of May and June, and fall, consisting of December.

5.2. Temperature and salinity

In the ECS shelf region the entire water column exhibits an evident seasonal thermal cycle (Figure 11a). A well developed thermocline is present down to 30-m depth in spring and extends to the bottom in summer. A significant cooling begins at the end of summer with weakening strength

with depth. The whole water column becomes well mixed with temperature near 18°C in autumn. This probably due to the entrainment mixing generated by strong surface winds, tidal mixing as well as strong surface buoyancy loss caused by net heat loss of 274 W/m² (Table 1) and fresh water loss of 13.3 cm/mon (Table 6). From autumn to winter the whole water column is uniformly cooled to 13° C. Total seasonal variability at the bottom is around 6.5°C. The surface salinity exhibits a minimum value of 32.88 ppt in spring, increases to 33.39 ppt in summer and further increases to its maximum value of 34.08 ppt in autumn, and then decreases to 33.74 ppt in winter (Figure 12a). From T-S diagram (Figure 13a) we can clearly recognize a seasonal layer of East China Sea Surface Water (ECSSW), which corresponds to relatively low salinities and high temperatures of summer, and an ECSDW layer, which is cooled and renewed in winter. From our data, the ECSDW (open circles in Figure 13a) has average characteristics of T = 12.82°C, S=33.88 ppt, $\sigma_t > 25.2$ kg/m³, which consists with an earlier study by Liu et al. [1992]. The surface freshness is in-phase with the surface fresh water flux F (Figure 7a) in such a way that the maximum (minimum) F and the lowest (highest) surface salinity occurs in the same season, spring (autumn). However, the surface dilution is off-phase with the Yangtze River water discharge. The lowest surface salinity (spring) does not occur at the same time as the maximum Yangtze River discharge. This may confirm an earlier study by Beardsley et al. (1985) that the summer fresh water discharge from the Yangtze River forms a relatively shallow, low salinity plume-like structure extending offshore on average towards the northeast. Thus, the dominant factor in determining near-surface salinity is the surface fresh water flux. Besides, a well developed halocline extends to 40-m in spring and summer, being stronger in spring.

In the YS basin the spring-summer thermocline is formed down to the bottom. The bottom water (Figures 11b and 12b) is observed as low temperature and moderately-high salinity water with a weak seasonal variation. The winter density, $\sigma_t > 25.6 \text{ kg/m}^3$. These values are consistent with many earlier studies [Lie, 1985; 1987; Li and Yuan, 1992; Chen et al., 1994] describing the characteristics of YSCW near the bottom all year round. The lack of seasonality might be due to the semi-enclosed basin and the bowl-type bottom topography (Figure 1) which limits mixing with the surrounding waters. The surface waters are freshest in summer ($S = 31.42 \text{ ppt}$) but rapidly achieve their saltiest condition in autumn (32.98 ppt). The net surface fresh water flux has the maximum value (4.84 cm/mon) in spring, reduces to a value of -1.96 cm/mon (computed from Table 7) in summer (July-November) and continue to drop to the minimum value of -7.96 cm/mon (Table 7) in autumn. Such a mismatch between surface salinity and F may suggest that the dominant factor for determining the near surface salinity structure in summer is the river run-off. This coincides with Chen et al.'s (1994) results based on hydrographic observations during 1986. From T-S diagram (Figure 13b) we can clearly recognize a seasonal variation of the YSCW, which is cooled and renewed in winter. We may define the YSCW having winter characteristics of $T = 6.5^\circ$, $S = 32.75 \text{ ppt}$, and $\sigma_t > 25.6 \text{ kg/m}^3$. These values are consistent with an earlier study by Liu et al. [1992].

In the CB region, there is a strong seasonal variation. A spring-summer thermohaline is present but weak (Figures 11c, 12c). From summer to autumn, a significant cooling takes place close to the surface and weakens with depth. The whole water column becomes well mixed with temperature near 17.0°C in autumn. In winter the whole water column is uniformly cooled to 14.3°C . Total seasonal thermal variability at the bottom is around 5.0°C . The surface salinity has a minimum value of 31.46 ppt in summer, increases to 33.99 ppt in autumn and further increases to the

maximum value of 34.41 ppt in winter, and then decreases to 32.68 ppt in spring (Figure 12c). Total seasonal haline variability at the bottom is around 1.69 ppt. Beardsley et al. (1985) indicates that the TWC bifurcates near the CB region into the Yellow Sea Warm Current and the Tsushima current. There should have some connection between the CB region and upper layer (30 m) of the TWC region. However, the similarity between CB and upper TWC profiles only occurs in temperature but not in salinity (Figures 11c and d). The seasonal surface salinity variation follows the seasonal cycle of F : minimum salinity and maximum surface fresh water flux in summer and vice versa in winter. From T-S diagram (Figure 13c) we can clearly recognize the TWC deep water (TWCDW) and YEMW.

In the TWC region the upper water column (surface to 60 m), usually called the TWC Upper Water (TWC UW), exhibits an evident seasonal thermohaline cycle (Figures 11d, 12d). Total seasonal variability of temperature (salinity) is around 7°C (1.02 ppt) at the surface and weakens with depth. Below 60 m depth there exists a permanent thermocline with very weak seasonal variation. At the bottom (150 m), the water properties are seasonally invariant; the temperature is about 15°C , and the salinity is around 34.62 ppt. In winter, the surface waters are cool with a temperature of 19°C . Significant warming begins in spring with a 4.0°C increase from winter conditions followed by a 3°C increase from spring to summer. In summer, the surface temperature reaches its maximum of 26.3°C . Significant cooling (4.7°C) occurs in autumn. The surface salinity has the minimum value of 33.67 ppt in summer, increases to the maximum value of 34.69 ppt in autumn and slightly decreases to 34.52 ppt in winter, and then decreases to 33.91 ppt in spring. The surface freshness is in-phase with the surface fresh water flux F (Figure 7d). From T-S diagram (Figure 13d) we can clearly recognize a seasonal layer of TWC, which corresponds relatively fresh and warm in summer and saline and cool in winter.

In the KC region the upper water column (surface to 80 m), usually called the Kuroshio Surface Water (KSW), exhibits an evident seasonal thermal cycle (Figures 11e,f; 12e,f). Total seasonal variability of temperature (salinity) is around 5.7°C (0.47 ppt) at the surface and weakens with depth. From 80 to 600 m there exists a permanent thermocline/halocline with very weak seasonal variation. At 1500 m depth, the temperature is about 3.7°C and the salinity is around 34.43 ppt. In winter, the surface has a minimum temperature (21.7°C). A significant warming begins in spring. There is a 3.7°C increase from winter to spring and a 2.0°C increase from spring to summer. In summer, the surface temperature reaches its maximum (27.4°C). A significant cooling starts in autumn. There is a 3.7°C decrease from summer to autumn. The surface salinity has the minimum value of 34.29 ppt in summer, increases to the maximum value of 34.75 ppt in winter, and then decreases to 34.56 ppt in spring. The surface freshness is in-phase with the surface fresh water flux F (Figure 7d). Our data also show existence of a S-type salinity profiles with a maximum salinity in the layer between 150 and 250 m, which is associated with the Kuroshio Sub-Surface Water (KSSW); and with a minimum salinity at 600 m depth, which is associated with the Kuroshio Intermediate Water (KIW). In the sublayer between 150 m and 450 m, the salinity decreases with depth. From T-S diagram (Figures 13e,f) we can clearly recognize a seasonal layer of KC, which corresponds relatively fresh and warm in summer and saline and cool in winter.

Putting five T-S diagrams (Figures 13a-e) into one T-S diagram, the five sub-regions and various ECS/YS water masses are well represented (Figure 14). We can see the connections and mixing of water masses among the five sub-regions. For example, the water masses in the CB region come from TWCDW, YEMW, and YSMW. The YS and ECS waters are mixed during spring and summer. Besides, various ECS/YS water masses are well classified on this T-S diagram.

6. Interannual Variability of Thermohaline Structure

Interannual variability of T , S features can be obtained by removing the seasonal signal. After removing the seasonal variability, we obtain the T , S anomalies. Figures 15-19 show the interannual variations of T , S at three different levels for each sub-region. Owing to the irregularity of the MOODS data, there might be no data in a given sub-region for some seasons. For example, there is no data in the YS in 1978 and 1985. We should be very cautious when interpreting the interannual variability from this data set.

In the ECS shelf region, the temperature anomaly has a maximum value of 3.4°C at the surface in spring 1980 and a minimum value of -3.3°C at the surface in spring 1979. The salinity anomaly has a maximum value of 1.87 ppt at the surface in spring 1977 and a minimum value of -1.78 ppt at the surface in spring 1984 (Figure 15). The modest ($|T_{\text{anomaly}}| > 2^{\circ}\text{C}$, $|S_{\text{anomaly}}| > 1$ ppt) and strong ($|T_{\text{anomaly}}| > 3^{\circ}\text{C}$, $|S_{\text{anomaly}}| > 1.5$ ppt) anomalies occur in spring and summer seasons (Tables 11-12). For example, a strong warming and salting process occurs in spring 1977, and a strong freshen and modest cooling process occurs in spring 1984.

In the YS region, the temperature anomaly has a maximum value of 6.0°C at 50 m depth in summer 1979 and a minimum value of -8.5°C at 20 m depth in summer 1984. The salinity anomaly has a maximum value of 1.03 ppt at the surface in spring 1976 and a minimum value of -2.84 ppt at the surface in spring 1982 (Figure 16). A strong freshen and modest warming process occurs in spring 1982 (Tables 8-9).

In the CB region, the temperature anomaly has a maximum value of 6.2°C at the 30 m depth in summer 1981 and a minimum value of -3.1°C at the surface in spring 1983. The salinity anomaly has a maximum value of 1.89 ppt at the surface in spring 1980 and a minimum value of -1.33 ppt at

the 30 m depth in summer 1977 (Figure 17). A very strong warming occurred in summer 1981 (Table 10). The years of 1970s were characterized as the freshen period and the years of 1980s were featured as the saline period (Table 11).

In the TWC region, the temperature anomaly has a maximum value of 3.0°C at 50 m depth in spring 1977 and a minimum value of -3.5°C at the surface in spring 1983. The salinity anomaly has a maximum value of 0.82 ppt at the surface in summer 1979 and a minimum value of -1.26 ppt at the surface in summer 1983 (Figure 18). The fluctuations of the salinity anomaly decreases with depth. Modest and strong anomaly periods are listed in Tables 12-13.

In the KC region, the temperature anomaly has a maximum value of 1.8°C at 150 m depth in autumn 1980 and a minimum value of -1.4°C at 50 m depth in winter 1986. The salinity anomaly has a maximum value of 0.23 ppt at 150 m depth in autumn 1975 and a minimum value of -0.35 ppt at the surface in summer 1982 (Figure 19). Modest and strong anomaly periods are listed in Tables 14-15.

7. Conclusions

The work presented here describes both climatological and interannual water mass structure of the East China and Yellow Seas. Based on the current system and bathymetry, we divided the area into five sub-regions: the East China Sea shelf, the Yellow Sea basin, the Cheju bifurcation zone, the Taiwan Warm Current area, and the Kuroshio Current area. We use the U.S. Navy's Master Oceanographic Observation Data Set and the Comprehensive Ocean-Atmosphere Data Set to investigate the linkage between the fluxes (momentum, heat, and moisture) across the air-ocean interface and the formation of the water mass features for the five sub-regions.

(1) The most important atmospheric forcing is the strong winter monsoon (north to northeast) and weak summer monsoon (southeast). The surface air temperature has a nearly latitudinal gradient with south-to-north difference of 18°C in February and 3°C in August. The surface relative humidity is generally higher in the summer season, mainly as a consequence of the southeast summer monsoon bringing moisture air from tropics. A relative humidity minimum (maximum) is present in all seasons near Kyushu Island (Chinese coast), which may lead to maximum (minimum) evaporation there.

(2) The air-sea heat budget at the surface is dominated by the incoming solar radiation balanced by latent and longwave heat energy loss. It was found that the Yellow Sea has an overall long term heat gain of 15 W m⁻² (caused by low latent heat flux), and the rest of the area has an overall heat loss of around 30 W/m² in the East China Sea and Cheju bifurcation zone, and of 65 W/m² in the Kuroshio and Taiwan Warm Current regions. The sensible heat flux is nearly zero in summer, which implies SST close to SAT. The monthly variation of net surface heat flux is nearly sinusoidal and quite similar among the five sub-areas. Q_{net} peaks in June in the Yellow Sea and in July in the rest of sub-areas.

(3) The air-sea fresh water budget exhibits a distinct winter fresh water loss and summer fresh water gain pattern. The whole area experiences an overall fresh water loss (1.8-4 cm/mon) at the surface.

(4) The East China and Yellow Seas do not follow the usual atmospheric seasons. We divided the four seasons based on the relative heat storage, namely, winter (January-April), spring (May-June), summer (July-November), and autumn (December).

(5) We have classified the water masses of the East China and Yellow Seas using climatological averages. The entire water column of the East China Sea shelf water and the Yellow

Sea (including the Cheju bifurcation zone) undergoes an evident seasonal thermal cycle with maximum values of temperature during summer and maximum mixed layer depths during winter. However, only the surface waters of the Taiwan Warm Current region (upper 60 m) and the Kuroshio region (upper 80 m) exhibit a seasonal thermal cycle. Below these depths, there is no evident seasonal variation.

(6) The salt balance of the surface layer is clearly affected by surface fresh water flux and river run-off. In the East China Sea shelf region, the surface freshness (low salinity) is in-phase with the surface fresh water flux ($P - E$) and off-phase with the Yangtze River water discharge. The lowest surface salinity (spring) does not occur at the same time as the maximum Yangtze River discharge (July). In the Yellow Sea, however, the surface freshness is off-phase with the surface fresh water flux and in-phase with the Yangtze River water discharge. Two different relations between surface salinity and Yangtze River run-off, off-phase in the East China Sea shelf and in-phase in the Yellow Sea, may confirm an earlier study by Beardsley et al. (1985) that the summer fresh water discharge from the Yangtze River forms a relatively shallow, low salinity plume-like structure extending offshore on average towards the northeast.

(7) The thermohaline structure of the East China Sea and Yellow Sea experiences a strong inter-annual variation. Among five sub-regions, the shallow areas (ECS, YS, CB, TWC) experience a larger interannual variation than the deep area (KC). During 1983-1984, a strong cooling and freshen period was found, especially in the Yellow Sea (-8.4°C temperature anomaly in 1984).

Acknowledgments

The authors are grateful to C.W. Fan at the Naval Postgraduate School for their programming assistance. This work was funded by the Naval Oceanographic Office, the Office of Naval Research NOMP Program, and the Naval Postgraduate School.

References

- Beardsley, R.C., R. Limeburner, H. Yu, and G.A. Cannon, Discharge of the Changjiang (Yangtze River) into the East China Sea. *Continental Shelf Res.*, 4, 57-76, 1985.
- Chen, C.S., R.C. Beardsley, R. Limeburner, and K. Kim, Comparison of winter and summer hydrographic observations in the Yellow and East China Seas and adjacent Kuroshio during 1986. *Continental Shelf Res.*, 14, 909-929, 1994.
- Chu, P.C., C.R. Fraclick, S.D. Haeger, and M.J. Carron, A parametric model for Yellow Sea thermal variability. *J. Geophys. Res.*, 102, 10499-10508, 1997a.
- Chu, P.C., S.K. Wells, S.D. Haeger, and M.J. Carron, Spatial and temporal scales of the Yellow Sea thermal variability. *J. Geophys. Res.*, 102, 5655-5668, 1997b.
- Chu, P.C., H.C. Tseng, C.P. Chang, and J.M. Chen, South China Sea warm pool detected in spring from the Navy's Master Oceanographic Observational Data Set (MOODS). *J. Geophys. Res.*, 102, 15761-15771, 1997c.
- Chu, P.C., Y.C. Chen, and S.H. Lu, On Haney-type surface thermal boundary conditions for ocean circulation models. *J. Phys. Oceanogr.*, 28, 890-901, 1998.
- Chu, P.C., S.H. Lu, and C.W. Fan, An air-ocean coupled nowcast/forecast system for the east Asian marginal seas. *Advances in Mathematical Modeling of Atmosphere and Ocean Dynamics*, Kluwer Scientific Publishing Co., in press, 2001.
- Elms, J.D., U.S. Navy regional climatic study of the central east Asian coast and associated waters. U.S. Naval Oceanography Command Report NAVAIR 50-1C-556, Stennis Space Center, Mississippi, 1990.

- Guan, B.-X., Patterns and structures of the currents in Bohai, Huanghai (Yellow Sea), and East China Sea. In: *Oceanology of China Seas*, Edited by D. Zhou et al., Kluwer Academic Publishers, Norwell, MA, 17-26, 1994.
- Hirose, N., H.-C. Lee, and J.-H. Yoon, Surface heat flux in the East China Sea and Yellow Sea. *J. Phys. Oceanogr.*, 29, 401-417, 1999.
- Hsueh, Y., Recent current observation in the Eastern Yellow Sea. *J. Geophys. Res.*, 19, 612-625, 1988.
- Langill, R.H., Forecasting guide for the Republic of Korea, Det. 18, 215 pp., 20th Weather Squadron, 1st Weather Wing, U.S. Air Force, San Francisco, Calif., 1976.
- Li, H. and Y. Yuan, On the formation and maintenance mechanisms of the cold water mass of the Yellow Sea. *Chinese J. Oceanol. Limnol.*, 10 (2) 97-106, 1992.
- Lie, H.-J., Wintertime temperature-salinity characteristics in the Southeastern Hwanghae (Yellow Sea). *J. Oceanogr. Soc. Japan*, 41, 291-298, 1985.
- Lie, H.-J., Summertime hydrographic features in the Southeastern Hwanghae (Yellow Sea). *Prog. Oceanogr.*, 17, 229-242, 1987.
- Liu, S., X. Shen, Y. Wang, and S. Han, Preliminary analysis of distribution and variation of perennial monthly mean water masses in the Bohai Sea, the Huanghai (Yellow) Sea and the East China Sea. *Acta Oceanol. Sinica*, 11, 483-498, 1992.
- Niino, H., and K.O. Emery, Sediments of shallow portions of East China Sea and South China Sea. *Geolog. Soc. Amer. Bull.*, 72, 731-762, 1961.
- Su, Y.-S., and X.-C. Weng, Water masses in China Seas. In: *Oceanology of China Seas*, Vol 1, edited by Zhou Di et al., Kluwer Academic Publishers, Boston, 3-16, 1994.

- Takahashi, S., and T. Yanagi, A numerical study on the formation of circulations in the Yellow Sea during summer. *La mer*, 33, 135-147, 1995.
- Van Loon, H. , Climates of the Oceans, *World Surv. Climatol*, 15, 453-458, 1984.
- Watts, I.E.M., Climates of China and Korea, *World Surv. Climatol.*, 8, 1-117, 1969.
- Yanagi, T. and S. Takahashi, Seasonal variation of circulations in the East China Sea and the Yellow Sea. *J. Oceanogr.*, 49, 503-520, 1993.
- Yanagi, T., and K. Inoue, Tide and tidal current in the Yellow/East China Seas. *La mer*, 32, 153-165, 1994.
- Yang, Z.S., J.D. Milliman, and M.G. Fitzgerald, Transfer of water and sediment from the Yangtze River to the East China Sea, June, 1980. *Canadian J. Fish. Aquatic Sci.*, 40, 72-82, 1983.

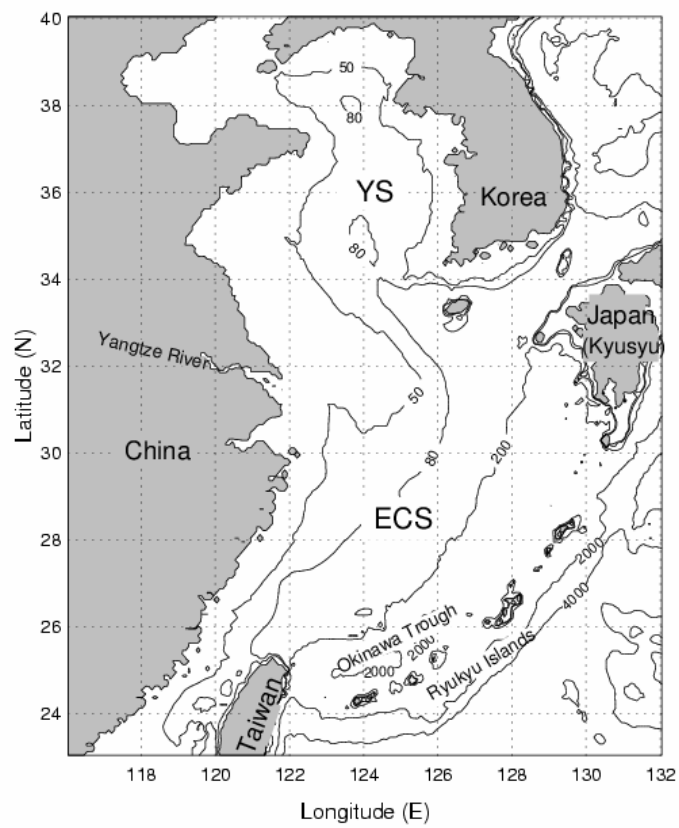


Figure 1. Topography and isobaths of the East China Sea and the Yellow Sea.

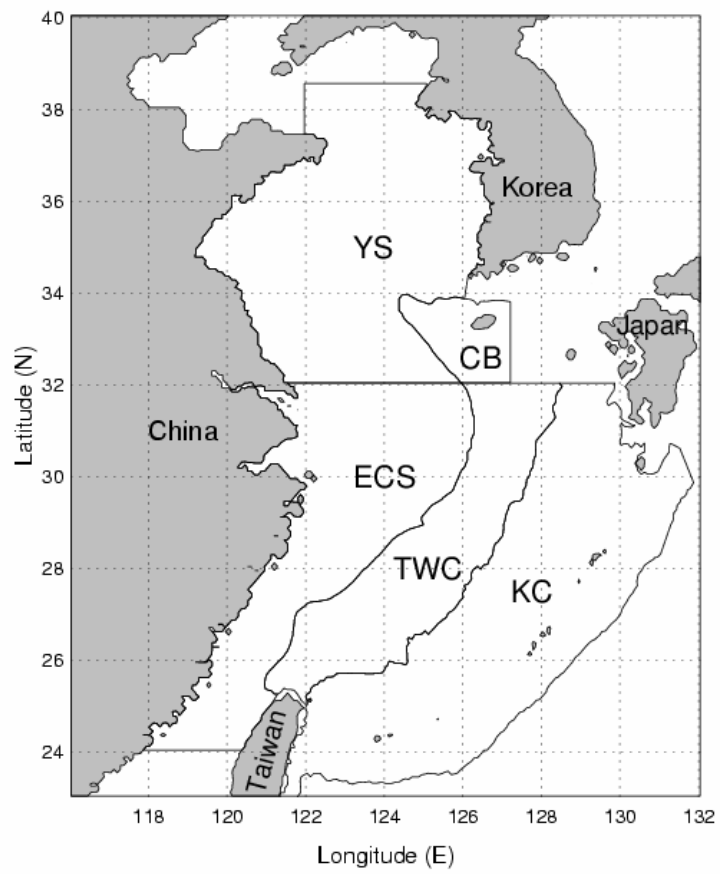


Figure 2. Subdivisions of ECS/YS.

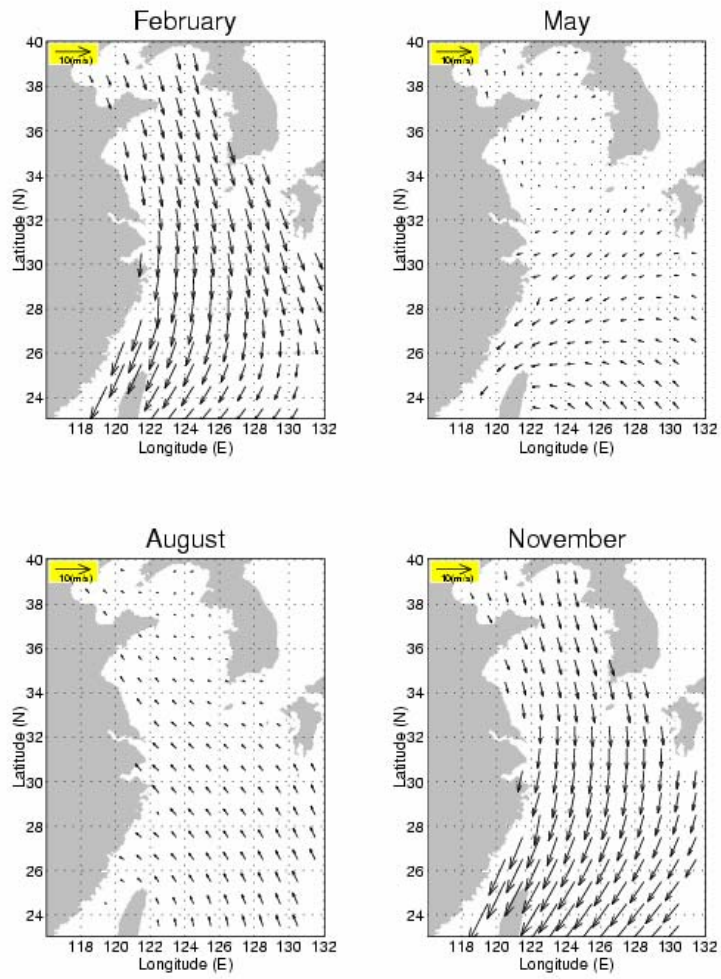


Figure 3a. Average surface winds for February, May, August and November from COADS.

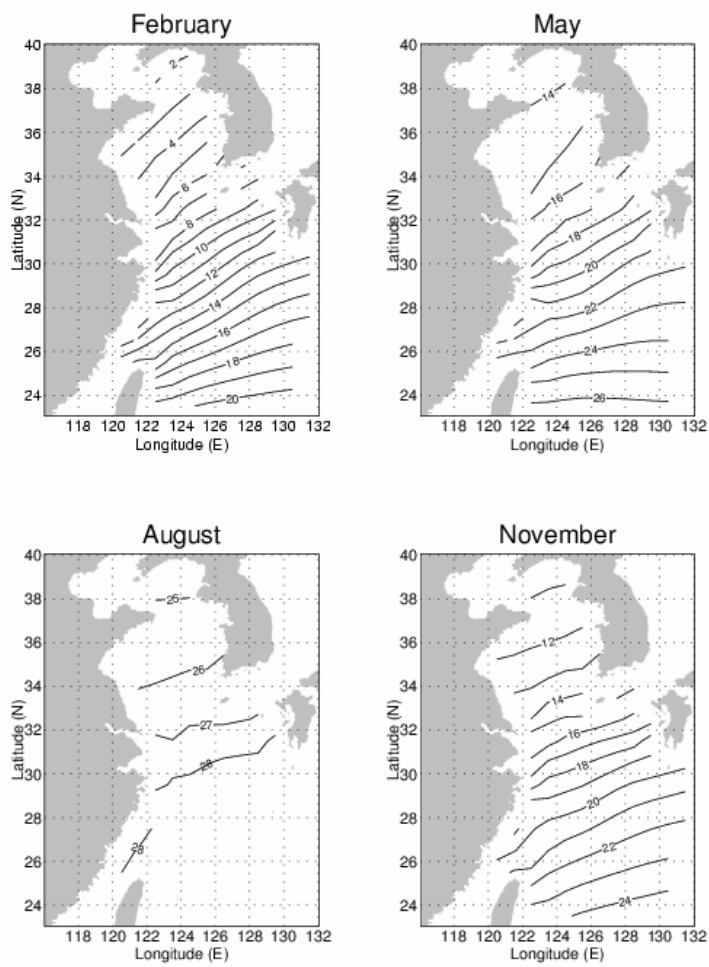


Figure 3b. Average surface air temperature ($^{\circ}\text{C}$) for February, May, August and November from COADS.

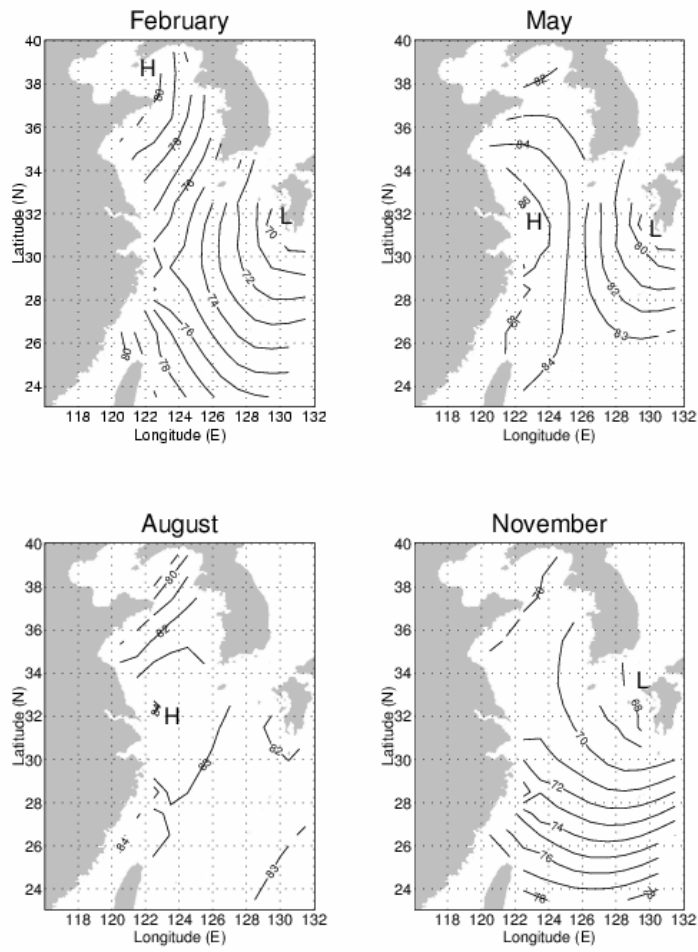


Figure 3c. Average surface relative humidity (%) for February, May, August and November from COADS.

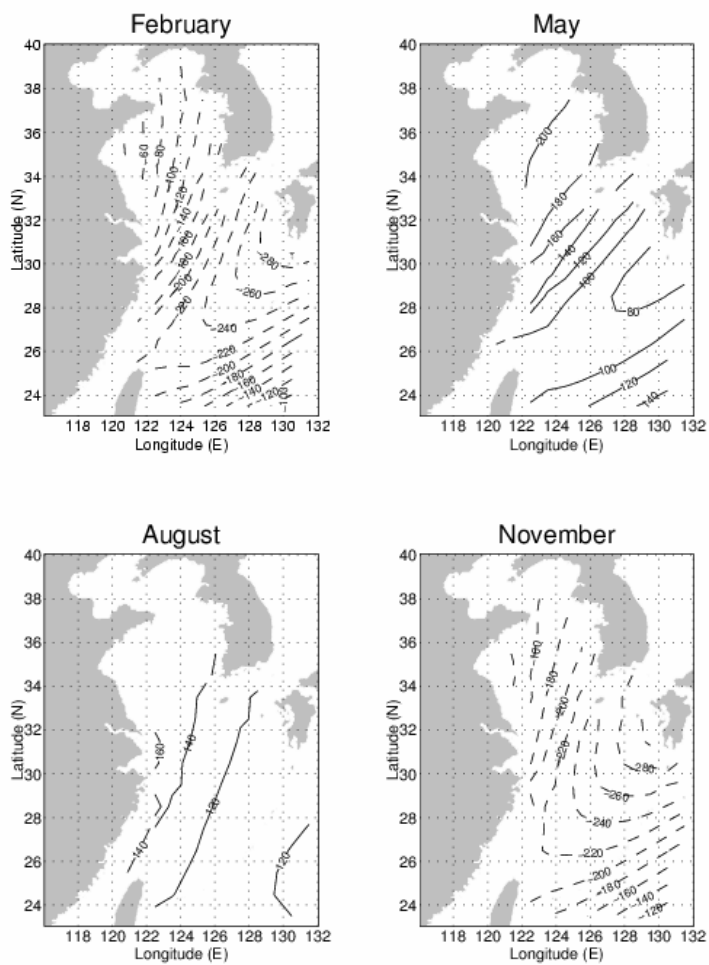


Figure 4. Average net surface heat flux (W/m^2) for February, May, August and November from COADS. Solid (dashed) lines indicate positive (negative) values.

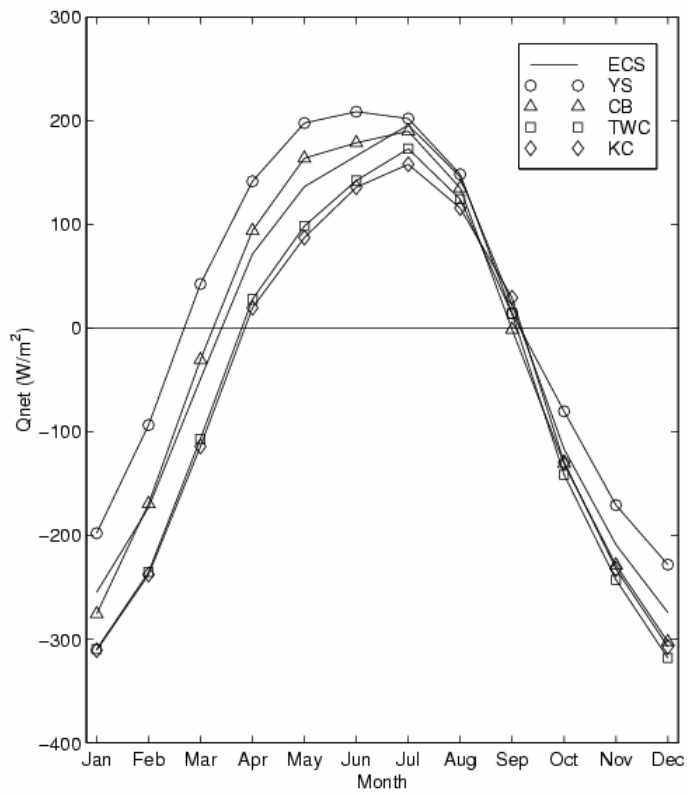


Figure 5. Seasonal variations of monthly mean net heat flux (W/m^2) for the five sub-regions.

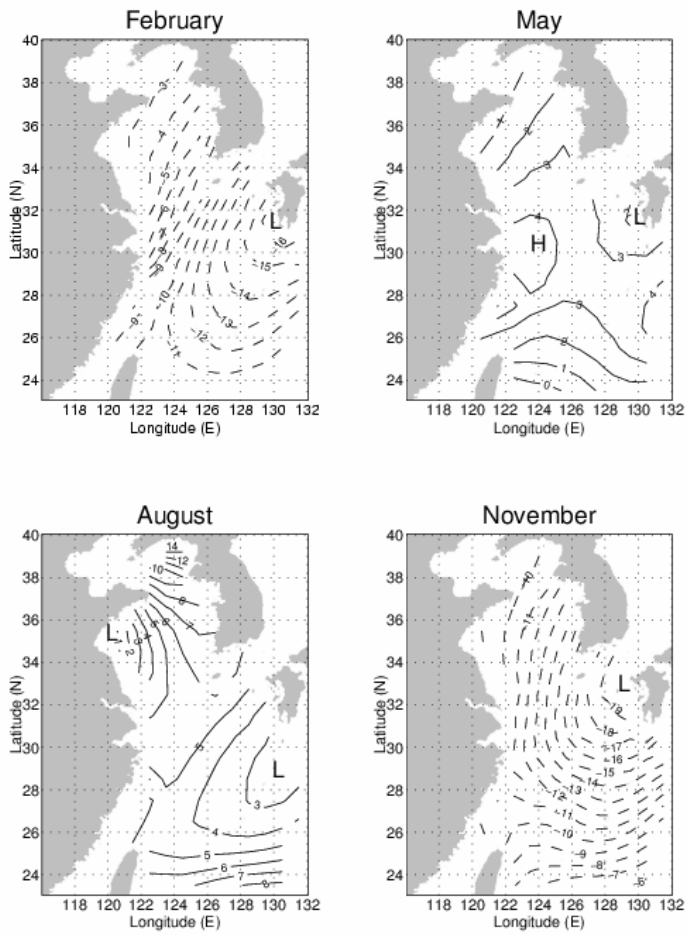


Figure 6. Average surface fresh water flux (cm/month) for February, May, August and November from COADS. Solid (dashed) curves indicate positive (negative) values.

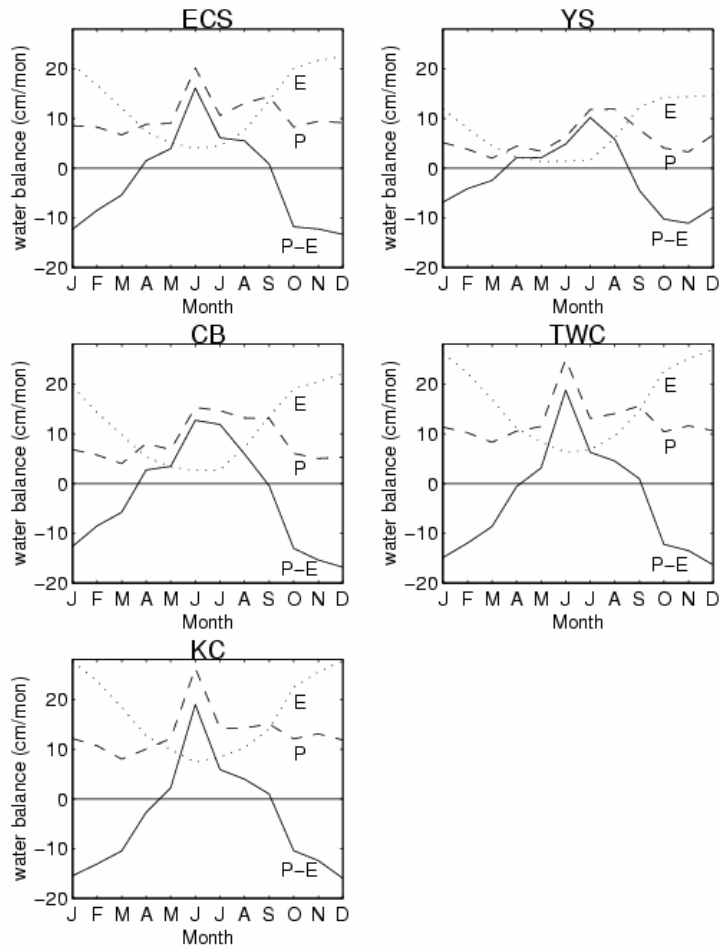


Figure 7. Seasonal variations of monthly mean fresh water flux (cm/month) for the five sub-regions.

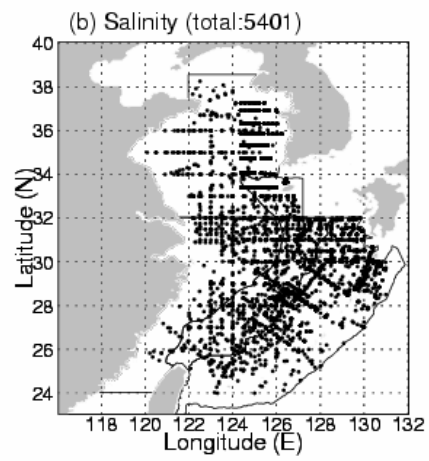
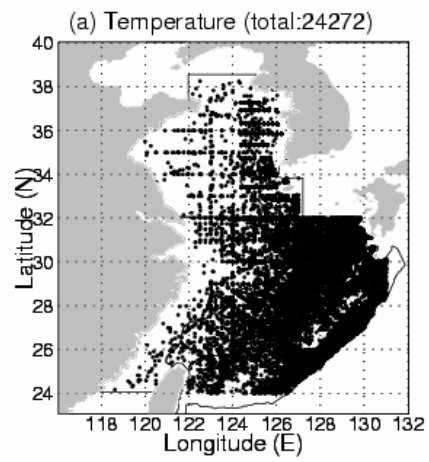


Figure 8. Spatial distribution of MOODS data during 1975-1986.

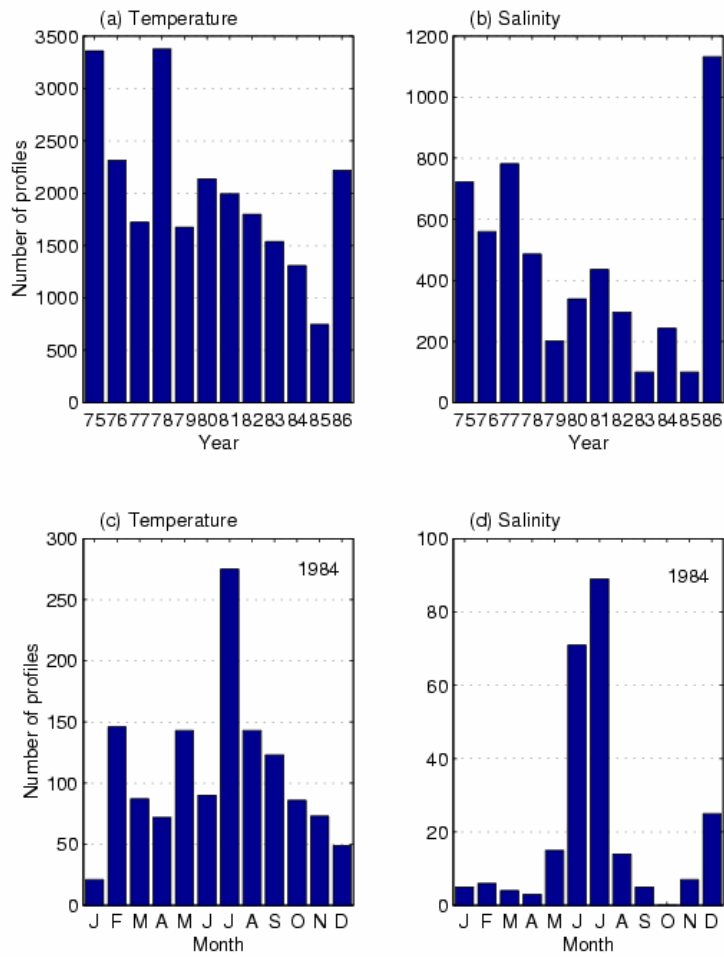


Figure 9. Temporally irregular cast distribution: (a) yearly temperature, (b) yearly salinity, (c) monthly temperature in 1984, and (d) monthly salinity in 1984.

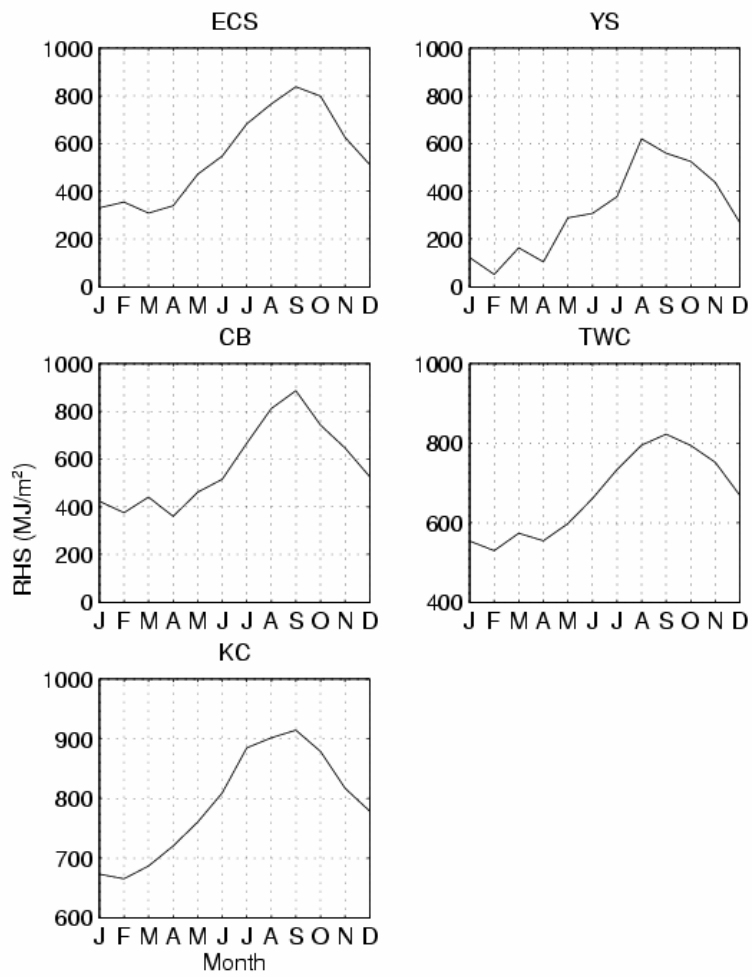


Figure 10. Seasonal variations of monthly mean relative heat storage for the five sub-regions.

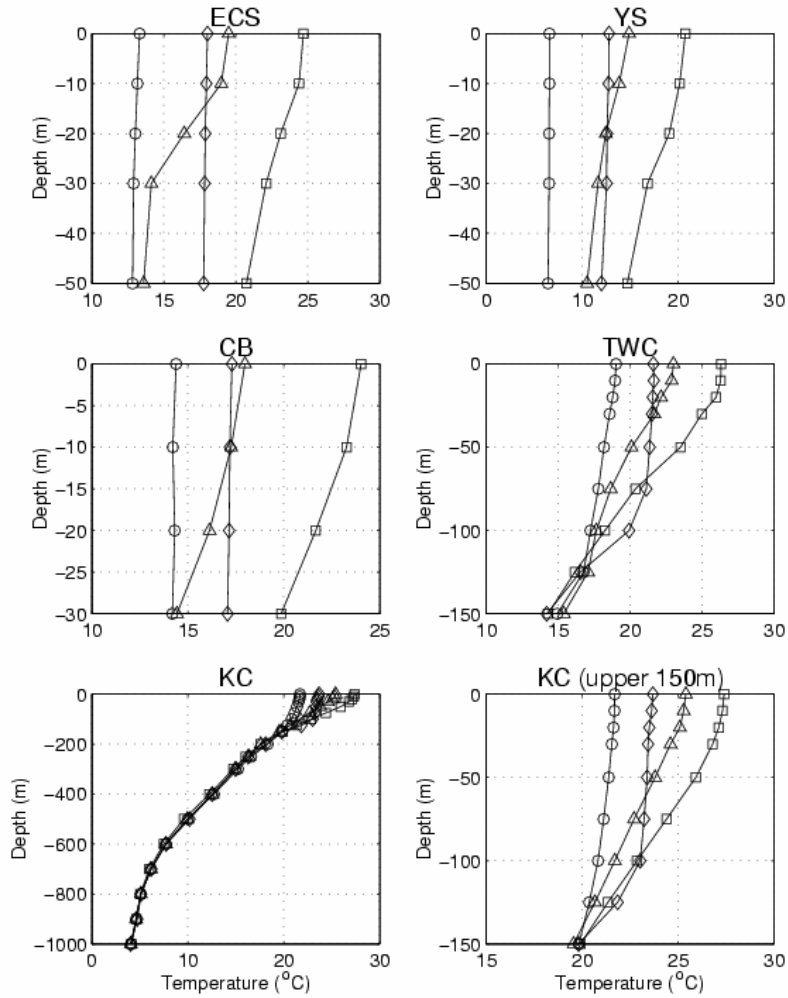


Figure 11. Seasonal climatological profiles of temperature for the five sub-regions: (a) the ECS shelf, (b) YS, (c) CB, (d) TWC, and (e) KC regions. The symbol 'o' denotes winter, 'Δ' denotes spring, '□' denotes summer and '◇' denotes fall.

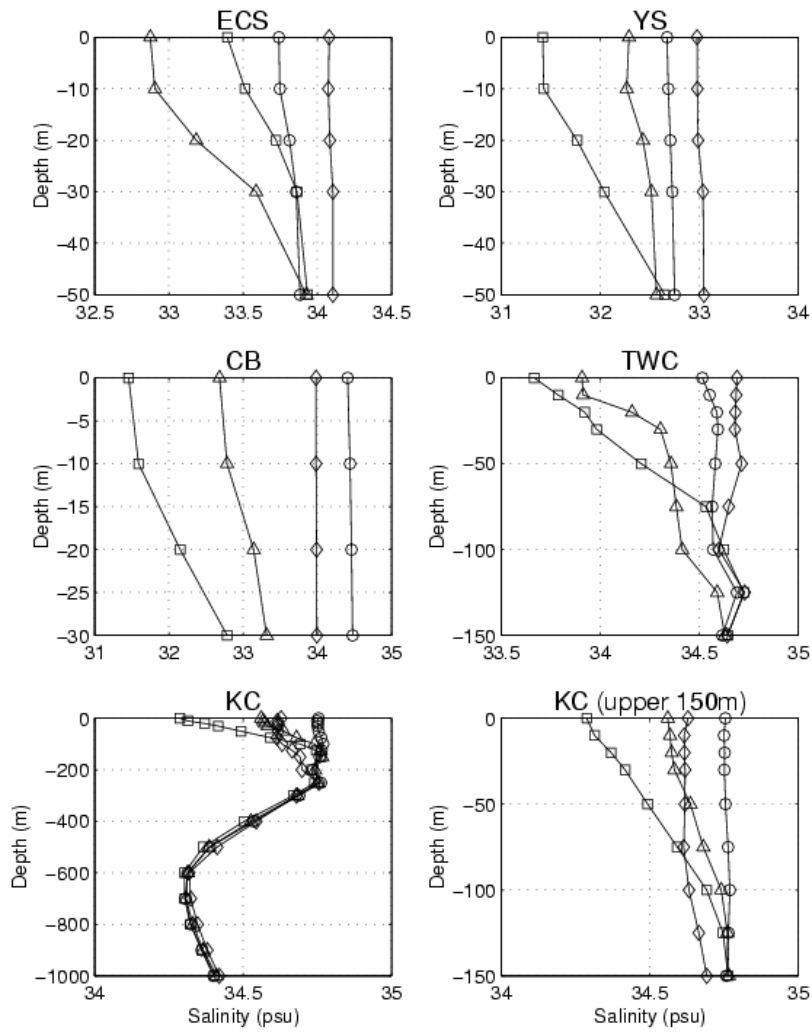


Figure 12. Same as Figure 14 except for salinity.

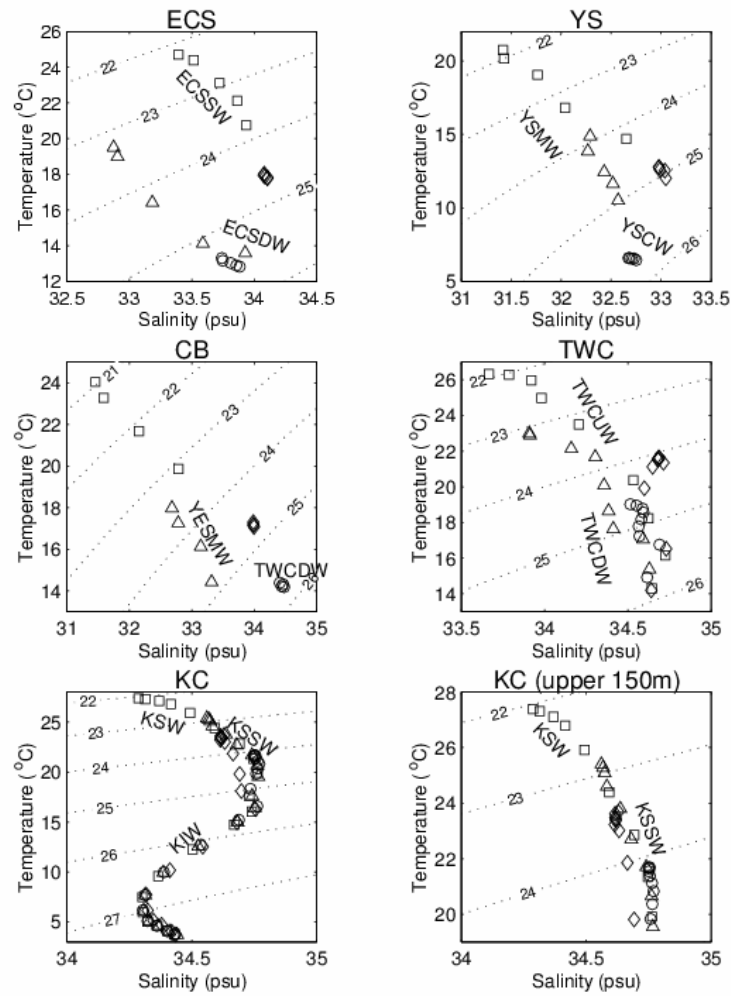


Figure 13. Seasonal climatological T-S diagrams for the five sub-regions: (a) the ECS shelf, (b) YS, (c) CB, (d) TWC, and (e) KC regions. The symbol 'o' denotes winter, ' Δ ' denotes spring, ' \square ' denotes summer and ' \diamond ' denotes fall.

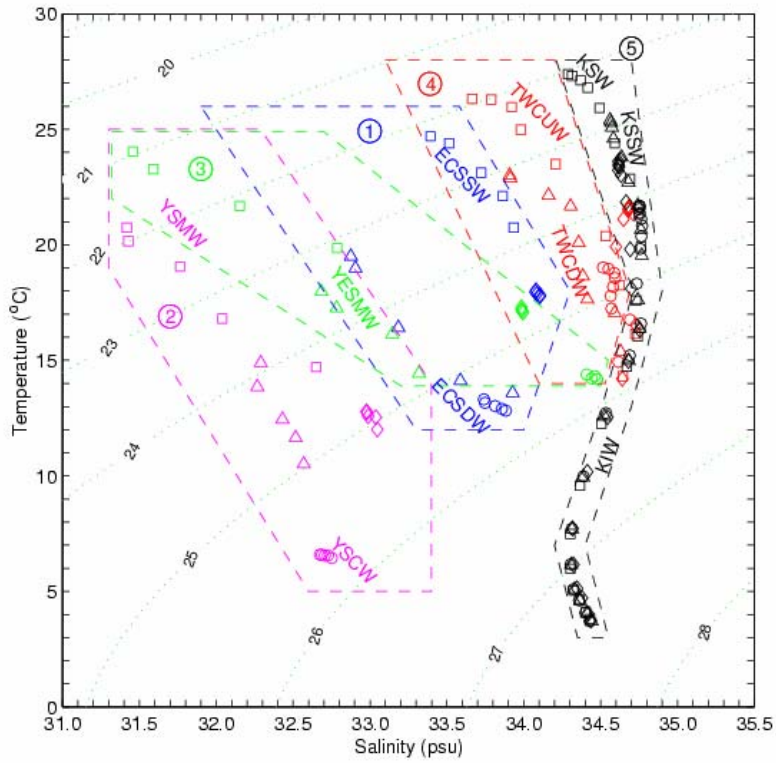


Figure 14. Water mass classification on climatological T-S diagram.

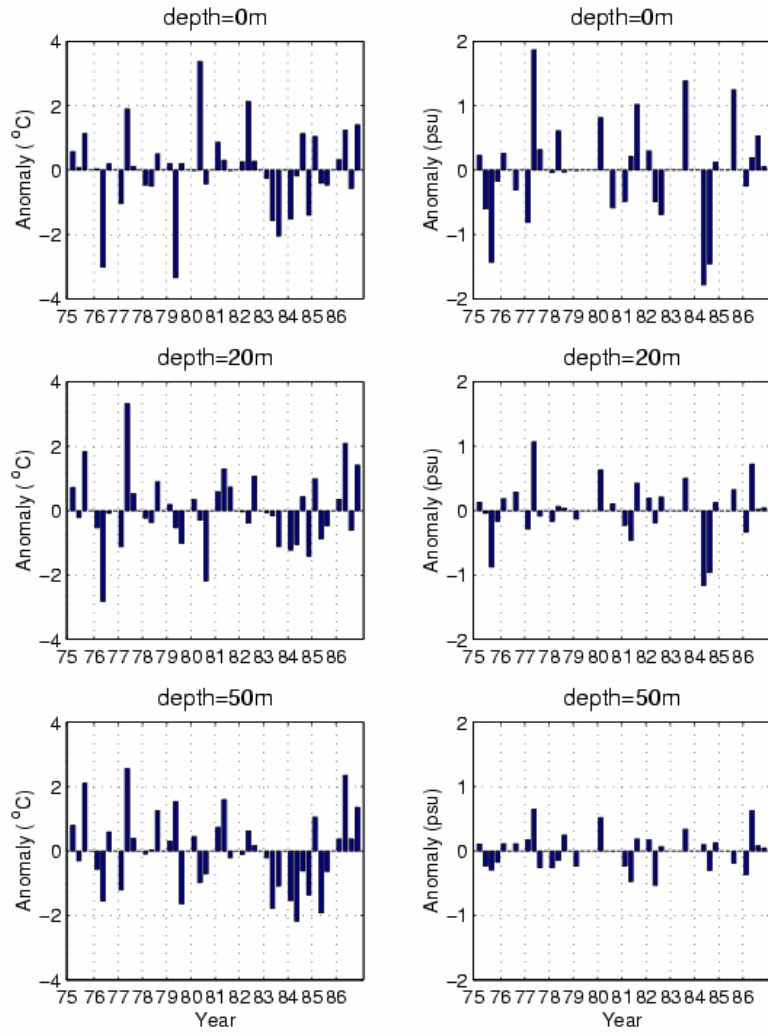


Figure 15. Interannual variation of temperature and salinity anomalies for the ECS shelf at different depths: (a) surface, (b) 20 m, and (c) 50 m.

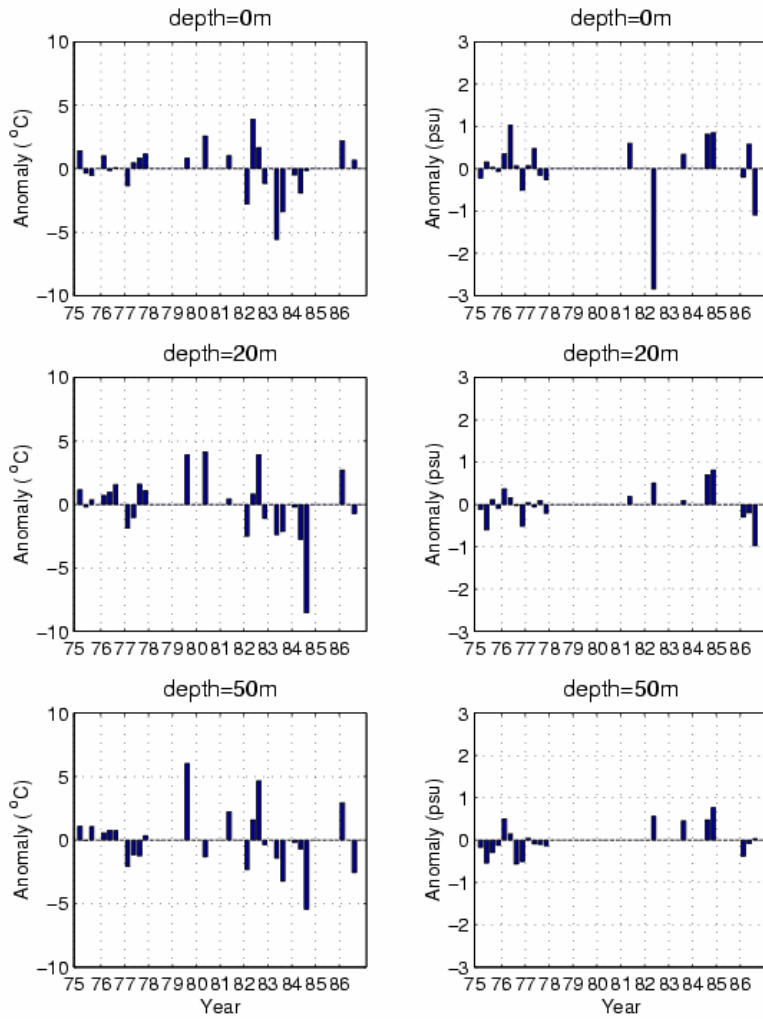


Figure 16. Interannual variation of temperature and salinity anomalies for the YS shelf at different depths: (a) surface, (b) 20 m, and (c) 50 m.

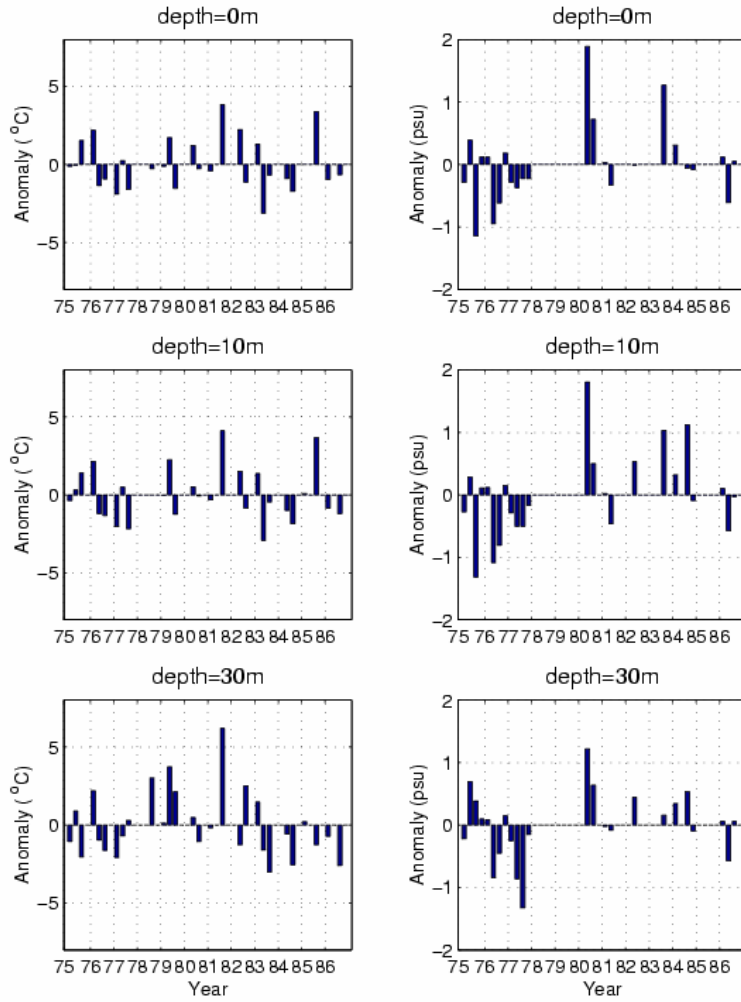


Figure 17. Interannual variation of temperature and salinity anomalies for the CB region at different depths: (a) surface, (b) 10 m, and (c) 30 m.

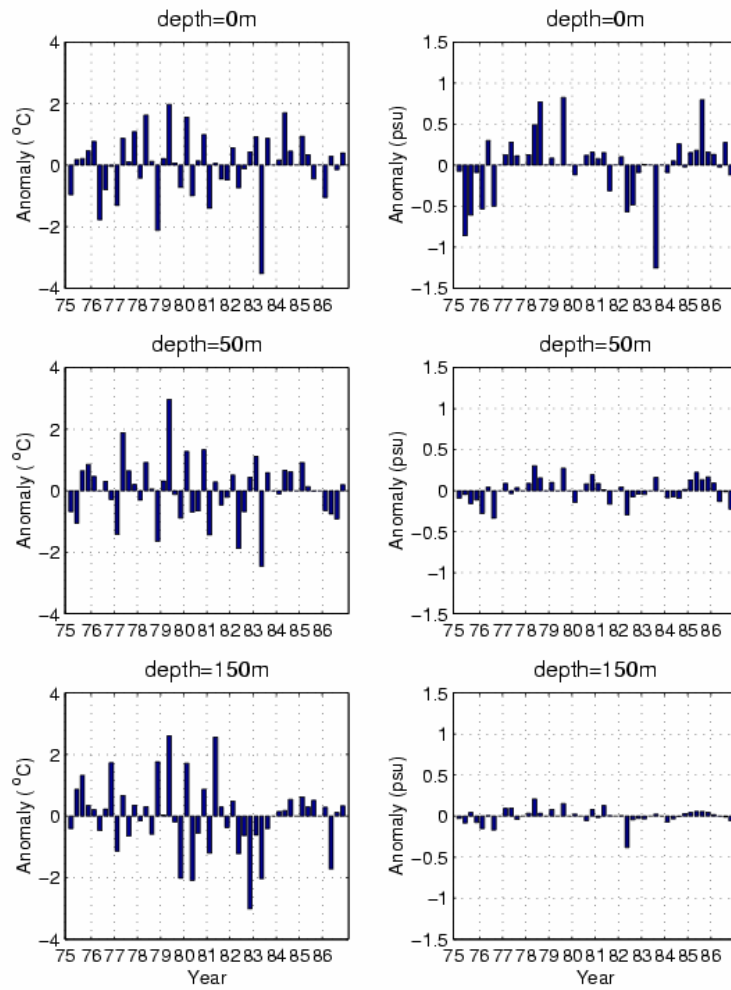


Figure 18. Interannual variation of temperature and salinity anomalies for the TWC region at different depths: (a) surface, (b) 50 m, and (c) 150 m.

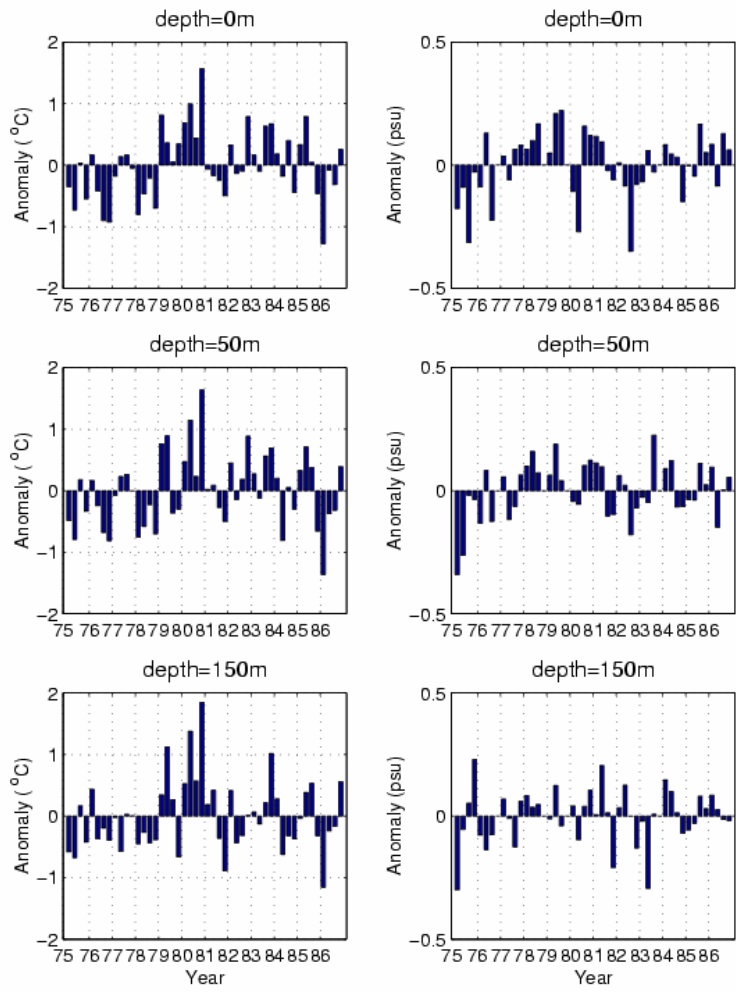


Figure 19. Interannual variation of temperature and salinity anomalies for the KC region at different depths: (a) surface, (b) 50 m, and (c) 150 m.

Table 1. Monthly surface heat flux components obtained from COADS data for the ECS shelf region.

Month	R_S (W/m ²)	R_L (W/m ²)	Q_S (W/m ²)	Q_L (W/m ²)	Q_{net} (W/m ²)	Q_S/Q_L
Jan	93.6	78.6	78.3	191.4	-254.8	0.41
Feb	122.0	71.4	64.3	159.3	-173.0	0.40
Mar	165.0	62.4	35.0	116.8	-49.2	0.30
Apr	208.0	51.5	14.0	70.8	71.3	0.20
May	234.8	43.5	5.4	49.5	136.4	0.11
Jun	241.2	34.3	1.5	39.4	166.0	0.04
Jul	269.7	33.1	-2.8	43.7	195.7	-0.06
Aug	257.4	38.4	0.1	72.8	146.1	0.00
Sep	207.5	47.9	8.1	128.6	22.8	0.06
Oct	158.5	62.0	22.4	190.5	-116.6	0.12
Nov	110.5	70.0	43.8	205.5	-208.9	0.21
Dec	89.0	79.3	71.6	212.0	-274.2	0.34
Annual Mean	179.7	56.1	28.5	123.4	-28.2	0.23

Table 2. Monthly surface heat flux components obtained from COADS data for the YS region.

Month	R_S (W/m ²)	R_L (W/m ²)	Q_S (W/m ²)	Q_L (W/m ²)	Q_{net} (W/m ²)	Q_S/Q_L
Jan	82.1	88.8	76.8	114.2	-197.7	0.67
Feb	117.6	79.1	53.3	78.7	-93.4	0.68
Mar	172.0	68.5	16.0	44.9	42.6	0.36
Apr	222.3	57.3	0.2	23.2	141.6	0.01
May	261.4	21.1	-1.0	13.6	197.7	-0.07
Jun	260.3	39.0	-1.7	14.4	208.6	-0.12
Jul	247.6	32.4	-2.6	15.8	202.0	-0.16
Aug	245.8	39.1	0.7	57.7	148.3	0.01
Sep	194.3	56.5	8.8	114.8	14.2	0.08
Oct	149.7	73.2	23.2	133.6	-80.3	0.17
Nov	99.7	84.6	48.2	137.6	-170.7	0.35
Dec	75.1	90.7	74.7	137.6	-228.0	0.54
Annual Mean	177.3	63.4	24.7	73.8	15.4	0.33

Table 3. Monthly surface heat flux components obtained from COADS data for the CB region.

Month	R_S (W/m ²)	R_L (W/m ²)	Q_S (W/m ²)	Q_L (W/m ²)	Q_{net} (W/m ²)	Q_S/Q_L
Jan	81.4	88.8	95.7	172.5	-275.6	0.55
Feb	116.6	79.2	70.8	136.1	-169.4	0.52
Mar	166.5	70.1	32.6	94.4	-30.5	0.35
Apr	212.1	57.0	10.0	51.2	93.9	0.20
May	248.0	48.8	2.9	32.4	163.8	0.09
Jun	241.1	36.0	1.6	24.9	178.5	0.06
Jul	247.2	32.0	-1.3	26.6	189.8	-0.05
Aug	245.4	38.8	2.7	68.7	135.1	0.04
Sep	190.7	51.8	12.4	127.9	-1.3	0.10
Oct	150.4	71.2	29.5	180.6	-130.9	0.16
Nov	103.2	83.7	56.0	192.0	-228.5	0.29
Dec	77.8	91.5	90.3	198.5	-302.5	0.45
Annual Mean	173.4	62.4	33.6	108.8	-31.5	0.31

Table 4. Monthly surface heat flux components obtained from COADS data for the TWC region.

Month	R_S (W/m ²)	R_L (W/m ²)	Q_S (W/m ²)	Q_L (W/m ²)	Q_{net} (W/m ²)	Q_S/Q_L
Jan	93.1	81.6	88.1	233.0	-309.7	0.38
Feb	120.5	74.4	74.3	207.1	-235.4	0.36
Mar	162.6	65.2	44.6	159.6	-106.8	0.28
Apr	206.1	53.7	20.3	104.2	27.9	0.19
May	230.2	44.4	9.9	77.5	98.3	0.13
Jun	238.0	34.6	4.2	57.2	142.1	0.07
Jul	269.9	34.5	-0.2	62.6	172.9	0.00
Aug	254.2	39.0	2.6	88.2	124.3	0.03
Sep	207.5	47.3	9.8	136.5	13.9	0.07
Oct	158.5	62.1	25.9	211.8	-141.3	0.12
Nov	110.9	70.4	47.4	235.6	-242.5	0.20
Dec	89.7	57.4	33.6	151.9	-64.5	0.18
Annual Mean	178.4	57.4	33.6	151.9	-64.5	0.18

Table 5. Monthly surface heat flux components obtained from COADS data for the KC region.

Month	R_S (W/m ²)	R_L (W/m ²)	Q_S (W/m ²)	Q_L (W/m ²)	Q_{net} (W/m ²)	Q_S/Q_L
Jan	99.4	80.5	81.4	248.0	-310.5	0.33
Feb	126.9	73.8	68.9	221.7	-237.6	0.31
Mar	168.5	65.3	43.4	173.9	-114.2	0.25
Apr	211.8	53.7	20.0	118.7	19.5	0.17
May	233.8	44.1	10.5	92.0	87.2	0.11
Jun	243.3	25.1	4.6	67.9	135.7	0.07
Jul	272.9	26.3	1.3	77.3	157.9	0.02
Aug	253.4	39.2	3.3	95.2	115.7	0.03
Sep	213.8	45.6	8.6	130.2	29.4	0.07
Oct	163.3	58.6	24.2	210.0	-129.5	0.12
Nov	116.3	66.7	42.7	238.8	-232.0	0.18
Dec	95.3	78.3	67.6	256.7	-307.2	0.26
Annual Mean	183.2	56.4	31.4	160.9	-65.5	0.20

Table 6. Warm and cold anomaly for ECS.

Anomaly Periods	Above 1°C	Above 1.5°C
Warm	Summer 1975 (50 m) Spring 1977 (20, 50 m) Spring 1980 (0 m) Spring 1982 (0 m) Spring 1986 (20, 50 m)	Spring 1977 (20 m) Spring 1980 (0 m)
Cold	Spring 1976 (0, 20 m) Spring 1979 (0 m) Summer 1980 (20 m) Summer 1983 (0 m) Spring 1984 (50 m)	Spring 1976 (0 m) Spring 1979 (0 m)

Table 7. Salty and fresh anomaly periods for ECS.

Anomaly Periods	Above 1 ppt	Above 1.5 ppt
Salty	Spring 1977 (0, 20 m) Summer 1981 (0 m) Summer 1983 (0 m) Summer 1985 (0 m)	Spring 1977 (0 m)
Fresh	Summer 1975 (0 m) Spring 1984 (0, 20 m) Summer 1984 (0 m)	Spring 1984 (0 m)

Table 8. Warm and cold anomaly for YS.

Anomaly Periods	Above 3°C	Above 5°C
Warm	Summer 1979 (20, 50 m) Summer 1980 (20 m) Spring 1982 (0 m) Summer 1982 (20, 50 m)	Summer 1979 (50 m)
Cold	Spring 1983 (0 m) Summer 1983 (0, 50 m) Summer 1984 (20, 50 m)	Spring 1983 (0 m) Summer 1984 (20, 50 m)

Table 9. Salty and fresh anomaly periods for YS.

Anomaly Periods	Above 1 ppt	Above 1.5 ppt
Salty	Spring 1976 (0 m)	
Fresh	Spring 1982 (0 m) Summer 1986 (0 m)	Spring 1982 (0 m)

Table 10. Warm and cold anomaly for CB.

Anomaly Periods	Above 2°C	Above 3°C
Warm	Winter 1976 (0, 10, 30 m) Summer 1978 (30 m) Summer 1979 (10, 30 m) Summer 1981 (0, 10, 30 m) Spring 1982 (0 m) Summer 1982 (30 m) Summer 1985 (0, 10 m)	Summer 1978 (30 m) Spring 1979 (30 m) Summer 1981 (0, 10, 30 m) Summer 1985 (0, 10 m)
Cold	Winter 1977 (10, 30 m) Summer 1977 (10 m) Spring 1983 (0, 10 m) Summer 1983 (30 m) Summer 1984 (30 m) Summer 1986 (30 m)	Spring 1983 (0 m) Summer 1983 (30 m)

Table 11. Salty and fresh anomaly periods for CB.

Anomaly Periods	Above 1 ppt	Above 1.5 ppt
Salty	Spring 1980 (0, 10, 30 m) Summer 1983 (0, 10 m) Summer 1984 (10 m)	Spring 1980 (0, 10 m)
Fresh	Spring 1975 (0, 10 m) Spring 1976 (10 m) Summer 1977 (30 m)	

Table 12. Warm and cold anomaly for TWC.

Anomaly Periods	Above 1°C	Above 1.5°C
Warm	Spring 1977 (0, 50 m) Winter 1980 (0, 50, 150 m) Winter 1983 (50 m)	Spring 1977 (0, 50 m) Winter 1980 (0, 150 m)
Cold	Winter 1977 (0, 50, 150 m) Summer 1977 (150 m) Winter 1981 (0, 50 m) Winter 1986 (0 m)	

Table 13. Salty and fresh anomaly periods for TWC.

Anomaly Periods	Above 0.5 ppt	Above 1.0 ppt
Salty	Summer 1978 (0 m) Summer 1979 (0 m) Summer 1985 (0 m)	
Fresh	Spring 1975 (0 m) Summer 1975 (0 m) Winter 1976 (0 m) Summer 1976 (0 m) Spring 1982 (0 m) Summer 1983 (0 m)	Summer 1983 (0 m)

Table 14. Warm and cold anomaly for KC.

Anomaly Periods	Above 1°C	Above 1.5°C
Warm	Spring 1979 (150 m) Spring 1980 (50, 150 m) Fall 1980 (0, 50, 150 m) Fall 1983 (150 m)	Fall 1980 (0, 50, 150 m)
Cold	Winter 1986 (0, 50, 150 m)	

Table 15. Salty and fresh anomaly periods for KC.

Anomaly Periods	Above 0.2 ppt	Above 0.3 ppt
Salty	Fall 1975 (150 m) Spring 1979 (0 m) Summer 1979 (0 m) Spring 1981 (150 m) Summer 1983 (50 m)	
Fresh	Winter 1975 (50, 150 m) Spring 1975 (50 m) Summer 1975 (0 m) Summer 1976 (0 m) Spring 1980 (0 m) Fall 1981 (150 m) Summer 1982 (0 m) Spring 1983 (150 m)	Winter 1975 (50 m) Summer 1982 (0 m)